

First-Principles Investigation of Photoisomeric Switching of Vibrational Heat Current across Molecular Junctions

G. Kurt^{ID} and H. Sevincli^{ID*}

*Department of Materials Science and Engineering, Izmir Institute of Technology, Gülbahçe Kampüsü,
35430 Urla, Izmir, Turkey*



(Received 23 July 2020; accepted 13 November 2020; published 15 December 2020)

Photoisomeric molecules rearrange their structure when exposed to light, which alters their chemical, electronic, mechanical, as well as vibrational properties. The present study explores the possibilities to tune the thermal transport across molecular junctions by using photoisomeric molecules. The effect of isomeric switching on phonon transport through single-molecule junctions linking two macroscopic reservoirs is investigated using density-functional-theory-based tight-binding calculations and Green-function formalism. The junctions are built using azobenzene and its derivatives (azobiphenyl and azotriphenyl) that display photoisomeric behavior. Effects of system setup on the heat current and the switching coefficient are studied systematically. Dependence on the molecular species, the choice of reservoir, as well as the type of linkers that bind the molecules to the reservoir are investigated with calculating the phonon-transmission spectra and temperature-dependent thermal conductance values. The results show that thermal conductance can be altered significantly by switching the molecule from *trans*- to *cis*-configuration since all molecules yield higher conductances in *trans*-configurations than their *cis*-configurations at temperatures higher than 50 K. In the low-temperature range, results reveal considerable switching coefficients exceeding 50%. At room temperature, the switching coefficient can be as high as 20%. It is shown that the effect is robust under the variation of both the molecular species and the linkers.

DOI: 10.1103/PhysRevApplied.14.064045

I. INTRODUCTION

Information-processing and energy-transfer technologies are based vastly on the control of electron flow. Phonons also carry energy and could, in principle, be used for information processing as well. Although living organisms can control thermal flux effectively, our control on phonon flow is relatively limited [1–6]. Finding out the ways of such efficient management has significant implications beyond scientific curiosity. The requirement for effective thermal management is rapidly increasing [7,8]. Taking control of thermal flux by the virtue of materials design is a significant step towards building thermal devices, which can even result in the development of a thermal counterpart of electronics [1,9–21].

An electronic switch is a well-established device that can turn the current from an “on” state to an almost completely “off” state. Similarly, a phononic thermal switch can act as a thermal modulator, which is achieved by alternating the heat current between two states. A possible implementation was shown by Sklan *et al.* via tuning the phonon band structure by light [22]. The switching of heat current across molecular junctions has been studied

in the literature. Ranganathan *et al.* analyzed the possibility of adjustable and reversible thermal conduction by virtue of photoisomerism and to that end by performing nonequilibrium molecular-dynamics simulations they calculated the thermal conduction of junctions built by using two different photoisomeric systems: azobenzene polymers and Spiropyran-Merocyanine isomers [23]. The results of this study suggest that controlling thermal conductance is rather difficult. Concurrently, Li and his coworkers proposed a theoretical thermal switch, which is composed of the molecular junction built by clamping a short alkane chain between graphene reservoirs [24]. When this junction is mechanically compressed, its thermal conductance drops by 50%. Royo *et al.* determined both the electronic and phononic transport properties of a graphene nanoribbon with a nanogap bridged by a stilbene molecule [25]. At low temperatures, phononic conductance can differentiate up to 70% upon a *trans-cis* conformational alternation that can be set mechanically or induced by photons of suitable wavelength. The reported *on:off* ratios of phononic switches are very low compared to that of electronic switches, and there is plenty of room for improvement.

Advances in measurement and fabrication techniques at the nanoscale made it possible to measure thermal transport across single-molecule junctions and to

*haldunsevincli@iyte.edu.tr

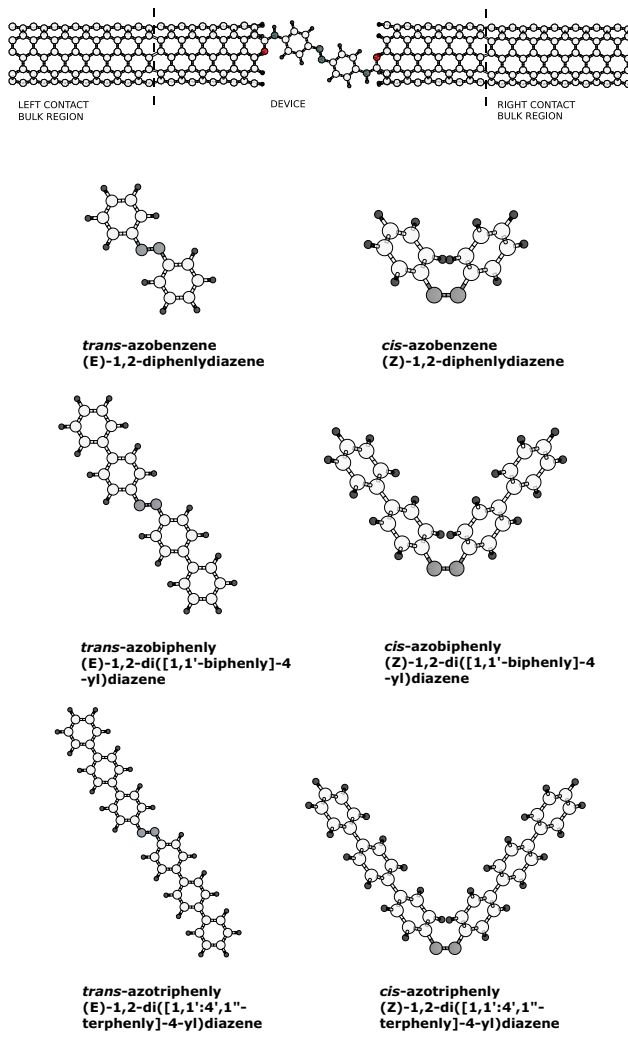


FIG. 1. Illustration of the molecular junction, partitions and the molecules. Molecules on the left illustrate the *trans*-isomers, those on the right illustrate the *cis*-isomers.

realize nanoscale thermal devices [26,27]. Photoisomeric molecules, whose spatial configuration can be altered by exposing to light, were shown to be useful in controlling the transport properties of molecular junctions [28]. The aim of the present study is to systematically investigate one of the building blocks of thermal devices, a thermal switch [29], based on photoisomeric molecular junctions. We use azobenzene and its derivatives that show photoisomeric behavior. The molecule is placed in between two coaxial semi-infinite carbon nanotubes (CNTs) to establish the junction (Fig. 1). The isomeric effect on azobenzene's thermal conductance, dependence on different molecular species, the influence of reservoir types, and the roles of linker groups are addressed.

The paper is organized as follows. The methods are summarized in Sec. II, structural aspects of the molecular junctions are explained in Sec. III, results and discussions

are presented in Sec. IV, and the last section is reserved for conclusions.

II. METHODS

The density-functional tight-binding (DFTB) method [30–33] is used as it is implemented in the DFTB+ software package [34]. DFTB is a fast and accurate method to determine chemical and physical properties of both bulk materials and molecular structures [35,36]. The calculations are performed using the mio-1-1 parameter set [37]. Self-consistent charge (SCC) calculation is performed with a tolerance of $10^{-7} E_h$. Broyden mixing is employed during SCC calculations with a mixing parameter of 1.5. Atomic coordinates are optimized using the conjugate gradient algorithm with a force tolerance of 0.02 eV/Å. Lattice parameters of the periodic parts are also optimized to reach the minimum energy configurations. The geometries of the structures and the energy differences between the isomers are further checked against and found to be consistent with density-functional-theory (DFT) computations (using both plane-wave [38,39] and localized-orbital [40] implementations) and the literature [41].

The DFTB method is combined with the Green-function (GF) method (see Refs. [42–44]), where the system is divided into three regions as the left reservoir (L), the right reservoir (R), and the device (D). The reservoirs are semi-infinite CNTs. An illustration of the molecular junctions and the partitions are given in Fig. 1(top). The device region is chosen in such a way that it can be simulated with periodic boundary conditions. It contains finite portions of the reservoirs so that its end atoms are replicas of a unit cell of the connected reservoir. Force constants are obtained from DFTB within the finite-difference approximation [45,46] and acoustic sum rule is employed [47].

The dynamical matrix of the partitioned system is of the form:

$$\Phi = \begin{pmatrix} \Phi^{LL} & \Phi^{LD} & \Phi^{LR} \\ \Phi^{DL} & \Phi^{DD} & \Phi^{DR} \\ \Phi^{RL} & \Phi^{RD} & \Phi^{RR} \end{pmatrix}. \quad (1)$$

It is assumed that there is no direct inter-reservoir coupling, that is all elements of Φ^{LR} and Φ^{RL} are zero. The uncoupled Green function of the parts are defined as $g^\alpha = [(\omega + i\eta)^2 - \Phi^{\alpha\alpha}]^{-1}$, with $\alpha = L, R$, or D and η is an infinitely small number. Self-energies due to coupling to the reservoirs are defined as $\Sigma^{L(R)} = \Phi^{DL(DR)} g^{L(R)} \Phi^{LD(RD)}$. Taking the couplings into account, the Green function of the device becomes $G^{DD}(\omega) = [(\omega + i\eta)^2 - \Phi^{DD} - \Sigma^L - \Sigma^R]^{-1}$. Phonon transmission is calculated as $\zeta(\omega) = \text{Trace}[\Gamma^L G^{DD} \Gamma^R G^{DD+}]$, where $\Gamma^{L(R)} = -2 \text{Im} [\Sigma^{L(R)}]$ stand for the broadenings. Assuming an infinitesimal temperature difference between

the reservoirs, thermal conductance is defined as

$$\kappa(T) = \int \frac{d\omega}{2\pi} \frac{\partial f_{\text{BE}}(\omega, T)}{\partial T} \hbar\omega\xi(\omega), \quad (2)$$

where f_{BE} is the Bose-Einstein distribution function. To determine the uncoupled surface Green functions of the reservoirs an iterative algorithm has been used [48]. Besides, a generic reservoir model is also implemented to easily predict the transport characteristics of a junction [44]. Since the sound velocity characterizes the acoustic phonons and acoustic phonons dominate the phononic thermal transport characteristics of a system, Green functions of the reservoirs are defined referring to the sound velocity at the reservoirs [44]. This scheme enables a fast and reasonably accurate calculation process. Details of the generic reservoir model is presented within the Supplemental Material [49]. Transmission and conductance values are calculated for *cis*- and *trans*-configurations of each system and the isomeric effect on thermal conductance is quantified as the switching coefficient, which is defined as

$$S = \frac{|\kappa_{\text{trans}} - \kappa_{\text{cis}}|}{\max(\kappa_{\text{trans}}, \kappa_{\text{cis}})} \times 100, \quad (3)$$

to quantify the efficiency of the system.

III. SYSTEMS

We investigate azobenzene and two of its derivatives, namely the 1,2-di([1,1'-biphenyl]-4-yl) diazene and 1,2-di([1,1':4',1"-terphenyl]-4-yl) diazene (to be referred to as azobiphenyl and azotriphenyl in this work) molecules, which transform between two isomeric states when exposed to radiation (Fig. 1). The motivation behind using different derivatives is to investigate the switching coefficient in molecules with similar structures but different lengths.

Trans-isomers are characterized by their planar structures, whereas the benzene rings of the *cis*-isomers are tilted with respect to each other (see Fig. 1). The planar geometry enables the *trans*-isomers to have π conjugation across the whole molecule while tilted shapes of *cis*-isomers disturb this conjugation. *Trans*-isomers are found to be energetically more stable than the *cis*-isomers. Energy differences between two isomeric states are around 0.2 eV for all three molecules. Dihedral angles are the CNNC angles between reciprocal benzene rings of *cis*-isomers and they characterize the isomeric switching. It is worthwhile to note that dihedral angles are approximately the same for all three molecules when they are free (see Table I).

Junctions are formed by connecting two CNT reservoirs with a single molecule (see Fig. 2). In this work, (5,5) armchair and (9,0) zigzag CNTs are used. The junction

TABLE I. Dihedral angles of *cis*-isomers measured in degrees.

	Free molecule	Linked to armchair CNT	Linked to zigzag CNT
Azobenzene	13.94	26.27	18.41
Azobiphenyl	13.42	18.56	15.17
Azotriphenyl	13.50	17.88	13.55

geometry can be expected to affect phonon transport considerably. Therefore, its details are investigated carefully, and summarized below for the cases of azobenzene.

The hydrogen atoms are removed from the *para* positions of azobenzene, and new bonds are formed by NH linker groups. NHCO groups are also considered in Sec. IV C to analyze the effect of linkers. The structures of the junctions should be the same to enable *cis*- and *trans*-isomers to transform to each other. With the addition of oxygen and carbon atoms, hexagons and pentagons are formed at the linking sites of armchair and zigzag CNTs, respectively (see Fig. 3). Two-coordinated carbon atoms at the ends of the CNTs are saturated with hydrogen.

Three periodic cells of pristine carbon nanotubes are fixed at both left and right ends of the device. The length of the junction (namely the separation between the reservoirs) is optimized by changing the separation exclusively, while relaxing the remaining atoms of the device region (see Supplemental Material for further details [49]).

IV. RESULTS AND DISCUSSIONS

For the free molecules, the energy differences between *trans*- and *cis*-isomers are 0.180, 0.202, and 0.203 eV for azobenzene, azobiphenyl, and azotriphenyl, respectively. When they are connected to CNT reservoirs, the energy differences show deviations. As a rule of thumb, the shorter the molecule is, the larger the deviation becomes. For azobenzene the energy difference is 0.305 eV (0.174 eV) for armchair-CNT (zigzag-CNT) reservoirs (see Fig. S1 within the Supplemental Material [49]). All remaining energy differences except for azotriphenyl with zigzag-CNT reservoirs rise moderately. When azotriphenyl is connected to zigzag CNT, the energy difference between its isomers falls to 0.1349 eV. It can be seen from Fig. 5(lower

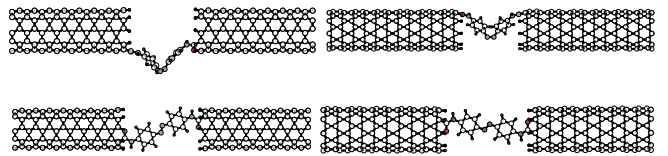


FIG. 2. Minimum energy geometries of azobenzene connected to armchair-CNT (zigzag-CNT) reservoirs are shown on the left (right). The upper (lower) configurations are the *cis*- (*trans*)-isomers.

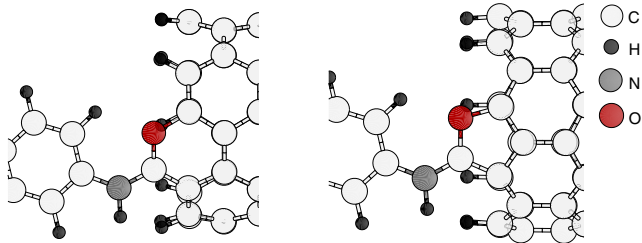


FIG. 3. Detailed structure of the junction at the linking site. Azobenzene is linked to armchair (left) and zigzag (right) CNTs via NH linkers.

panel) that the planar geometry of *trans*-azotriphenyl is considerably deformed when connected to zigzag CNT. Consequently, the energy difference is lowered. The junctions with *trans*-states are energetically more stable than *cis*-states for all molecules.

A. Isomeric switching with azobenzene

In this section, we investigate the effect of isomeric switching on thermal conductance of junctions built using azobenzene. Junction geometries are illustrated in Fig. 2. The structures on the left (right) have armchair-CNT (zigzag-CNT) reservoirs, and the upper (lower) structures belong to *cis*- (*trans*-) isomeric states. Despite the differences in geometrical orientations, the bending angles, namely the C-N-C angles where one carbon atom belongs to the CNT, the nitrogen atom belongs to the linker, and the other carbon atom is located at the *para* position of the benzene, are quite similar. For the armchair-CNT reservoirs, the right and left angles are quite similar and approximately equal to 124° . There is a slight difference at the left and right sides for the zigzag-CNT case, which is mainly because of the difference in the relative position of the left (right) linking site with respect to the tube axis. The left and the right angles are 124.72° and 125.16° , respectively.

Thermal conductance and the switching coefficient of azobenzene junctions are shown in Fig. 4 as functions of temperature. We use a color code in all conductance and switching coefficient plots. Namely, blue and red curves are for reservoirs of armchair-CNT and zigzag-CNT, respectively. Dark (light) colors distinguish the molecules in their *trans*- (*cis*-) configurations. At finite temperatures, it is observed that systems with armchair-CNTs have higher κ values than those with zigzag CNTs. It can be seen from the transmission spectra of azobenzene molecules linked to different reservoirs that armchair CNTs yield higher transmission at almost all frequencies (Fig. 7). We should note that the reduction in conductance when zigzag CNT is used in place of armchair CNT is not related to the thermal conductances of the CNTs. Room-temperature conductance values of pristine armchair and zigzag CNTs are found as 2.8774 nW/K and 2.7944 nW/K , respectively, which are consistent with

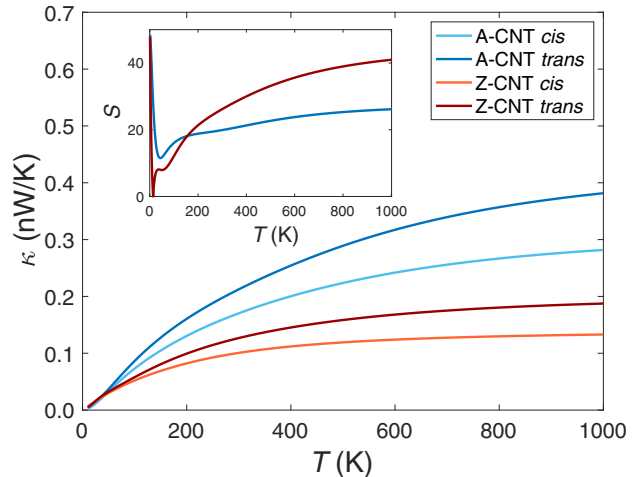


FIG. 4. Conductance values of azobenzene junctions. Blue and red curves are for armchair and zigzag CNTs, respectively. Dark (light) colors distinguish the *trans*- (*cis*-) configurations. The inset shows the corresponding switching coefficients.

the previous literature [50]. The main reason for the conductance differences between armchair- and zigzag-CNT reservoirs is the geometrical features of the junctions. In armchair-CNT junctions, a hexagon is formed at the linking site, whereas a pentagon is formed in zigzag-CNT junctions (see Fig. 3). The difference is not only in the number of bonds, but also the bond angles and the orientation of the molecule with respect to the tube axis are changed. As a result, dihedral angles differ considerably for different CNTs.

For a given reservoir type, *trans*-azobenzene has higher κ values at all temperatures except for those lower than approximately 50 K. The weight factor $\hbar\omega\partial_T f_{\text{BE}}$ eliminates contributions from the states with frequency higher than 2 THz at 10 K. This filtering is realized for $\nu > 10 \text{ THz}$ at 50 K. At such low temperatures, small differences in transmission spectrum result in considerable differences in conductances. Consequently, S values are around 50% at low temperatures. As temperature rises, S values drop suddenly with the contribution of higher-energy modes. For zigzag CNT, S is equal to zero at around 20 K, then it starts to rise. At temperatures below 20 K, *cis*-isomeric states are more conductive than *trans*-isomeric states. Since the *trans*-isomer is more conductive above 20 K, the switching coefficient drops to zero for junctions with a zigzag-CNT reservoir. However, for the armchair-CNT case, *trans*-isomeric states are more conductive than *cis*-isomeric states at all temperatures, and S is always finite. The switching coefficient for armchair-CNT reservoirs is 19.81% while it is 20.58% for the zigzag-CNT reservoirs at 300 K. A relevant point to mention here is that the switching coefficients for different reservoirs are close at temperatures below room temperature, even though conductance values are rather different. However,

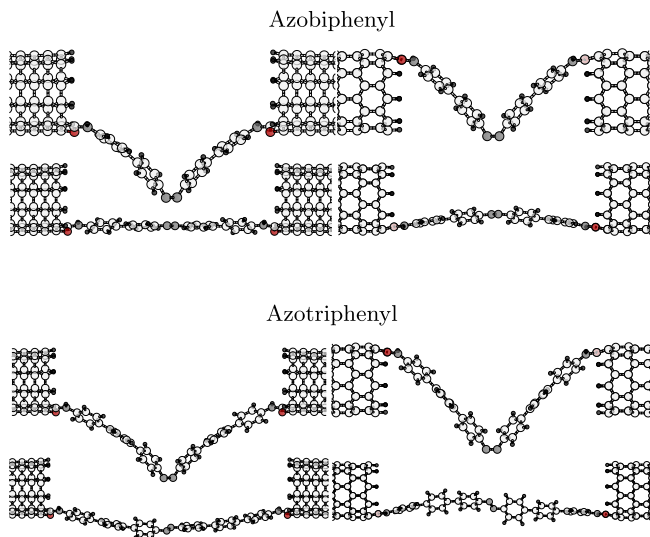


FIG. 5. (Upper panel) Junction geometries of *cis*- (*trans*-) azobiphenyl molecules between armchair- (left) and zigzag- CNT (right) reservoirs. (Lower panel) *cis*- (*trans*-) azotriphenyl between armchair (left) and zigzag (right) CNTs.

at high temperatures S values for zigzag CNT are higher than those for armchair CNT. The incomplete folding of the *cis*-isomer when connected to armchair CNT lowers the S value.

B. Effects of different molecular species and reservoir types

In this section, dependence of the switching coefficient on the type of isomeric molecule is investigated. For this purpose, junctions are constructed using two derivatives of azobenzene, namely azobiphenyl and azotriphenyl (Fig. 5). Temperature-dependent thermal conductances and switching coefficients are plotted in Fig. 6. It is clear that when a molecule is in *trans*-state, its conductivity is higher from its *cis*-state, independent of the species of the molecule. This is valid at temperatures above 50 K. At temperatures below 50 K, S increases with the molecule's length. However, at temperatures higher than 50 K, S decreases with increasing length.

Table II summarizes the switching coefficients (S) and conductances at 300 K. One observes that S is highest for the shortest molecule (azobenzene) and lowest for azotriphenyl independent of the type of reservoir. S for azobiphenyl is close to that of azobenzene for armchair CNT but it is close to that of azotriphenyl for zigzag CNT. This behavior can be understood by examining the junction geometries, which are illustrated in Fig. 5 (upper panel). *Trans*-azobiphenyl preserves its planar geometry when connected to an armchair CNT but the geometry is largely disturbed and the molecule is bent when connected to a zigzag CNT. Therefore, κ_{trans} and S are reduced. The

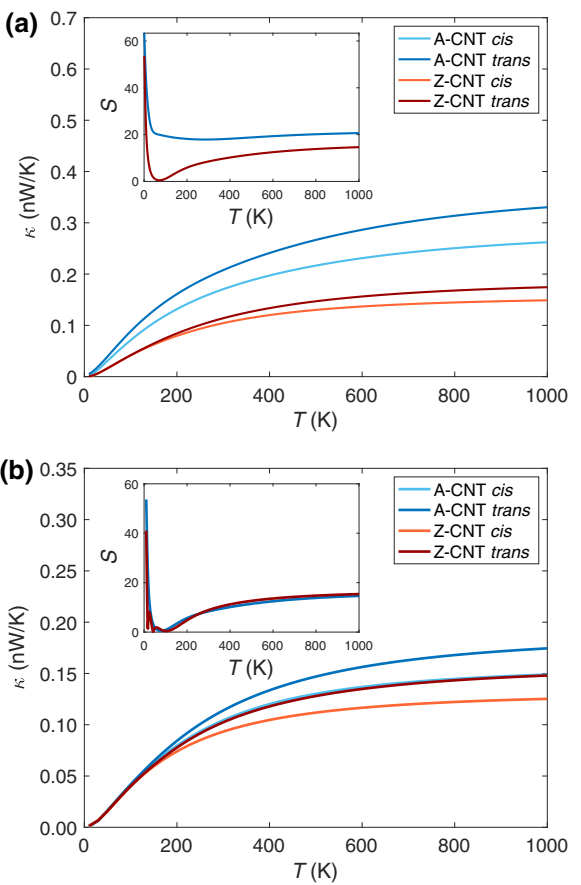


FIG. 6. Temperature-dependent conductance for junctions of azobiphenyl (a) and azotriphenyl (b) molecules using armchair- (blue) and zigzag-CNT (red) reservoirs. Lighter (darker) colors indicate the *cis*- (*trans*-) configurations. The insets show the corresponding switching coefficients.

disturbed geometries remain even after the junction separation is optimized. Since bending of azobiphenyl is specific to zigzag CNT only, we deduce that bending is due to the difference in bonding geometry at the linking site of the CNT atoms.

Geometrical disturbances are observed in azotriphenyl junctions too (see lower panel of Fig. 5). Benzene rings

TABLE II. Thermal conductances and switching coefficients of considered systems at 300 K.

Reservoir	Molecule	κ_{cis} (nW/K)	κ_{trans} (nW/K)	S
Armchair CNT	Azobenzene	0.1704	0.2125	19.81%
	Azobiphenyl	0.1706	0.2078	17.90%
	Azotriphenyl	0.1044	0.1144	8.74 %
Zigzag CNT	Azobenzene	0.1007	0.1268	20.58%
	Azobiphenyl	0.1044	0.1154	9.53%
	Azotriphenyl	0.9330	0.1024	8.11%
Generic	Azobenzene	0.1993	0.3056	34.78%

rotate with respect to each other in both *trans*- and *cis*-configurations, which is an additional factor to reduce thermal conductance. These disturbances suppress conductance of both isomers with either reservoir types and the switching coefficient is reduced.

In the azobenzene case, since the molecule is short, folding of the *cis*-isomer is not completely achieved and the switching coefficient is lower than expected. The C-N-N-C dihedral angles of *cis*-isomers are shown in Table I. The most significant change happens in azobenzene with armchair CNT, where the dihedral angle for *cis*-azotripenly with zigzag-CNT reservoirs stays approximately equal to that of the free molecule. One can expect the extended molecules to compensate these deviations at the linking site. However, structural disturbances become more substantial in determining their conductance.

In order to distinguish the geometrical effects arising from coupling to reservoirs, we implement “generic reservoirs,” which are characterized by the speed of sound at the reservoirs (see Ref. [44]) They also enable us to

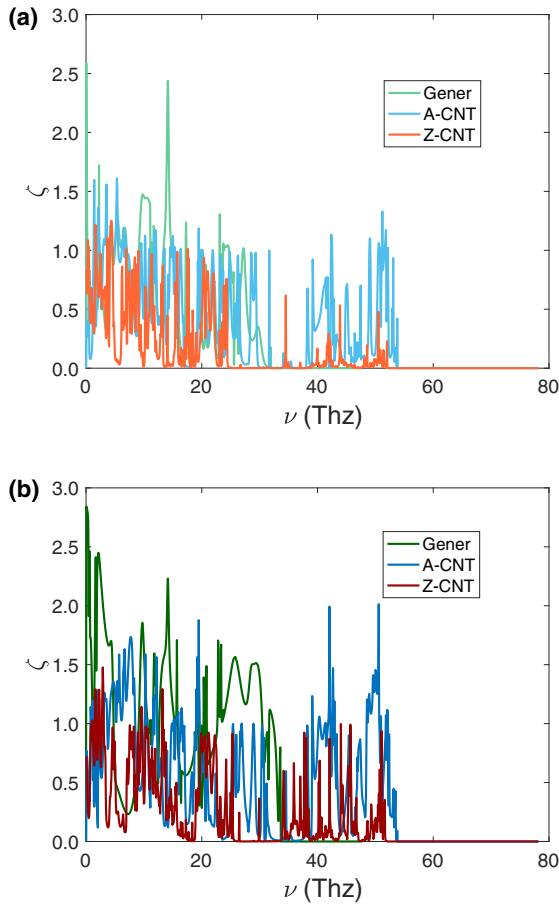


FIG. 7. Transmission spectra of azobenzene isomers linked to armchair-CNT, zigzag-CNT, and generic reservoirs. (a) transmission spectra of *cis*- (b) (*trans*)-isomers linked to different reservoirs. Red (green) curves are for zigzag (generic) reservoirs, and blue lines indicate armchair reservoirs.

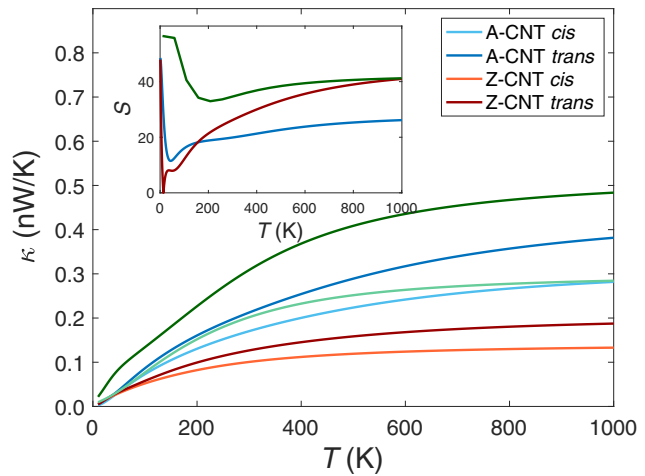


FIG. 8. Conductances of azobenzene isomers with different reservoirs. Red, blue, and green curves stand for armchair-CNT, zigzag-CNT, and generic reservoirs, respectively. Darker (lighter) colors are for *trans*- (*cis*)-configurations. The corresponding switching coefficients are shown in the inset.

check whether the observed effects are specific to CNT reservoirs, or generalizable. Here, we implement generic reservoirs that support only the acoustic modes. The sound velocities of different polarizations can be chosen independently. We choose them to be identical for the sake of simplicity and set to 15 km/s, which is the average of group velocities for LA and TA modes in a (10,10) CNT. The force constant between the generic reservoir and the molecule is set equal to the first-nearest-neighbor force constant of the generic reservoir. The coupling takes place between the end atom of the otherwise free molecule, hence the magnitude of thermal switching in the absence of geometrical disturbances can be calculated.

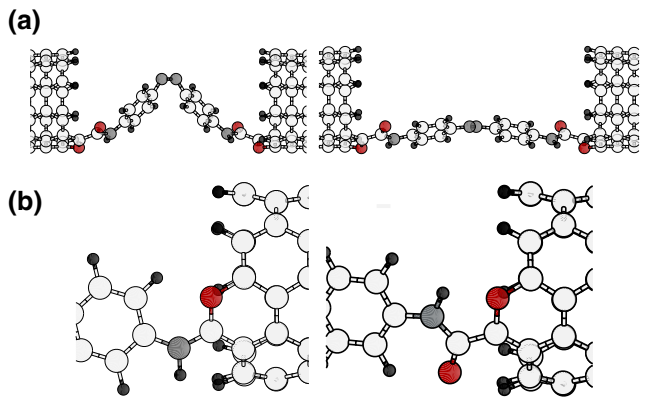


FIG. 9. (a) Junctions of *cis*- and *trans*-azobiphenyl linked to armchair CNT by NHCO linkers, left and right, respectively. (b) Closeups of NH (left) and NHCO (right) linkers binding the molecule to armchair CNTs.

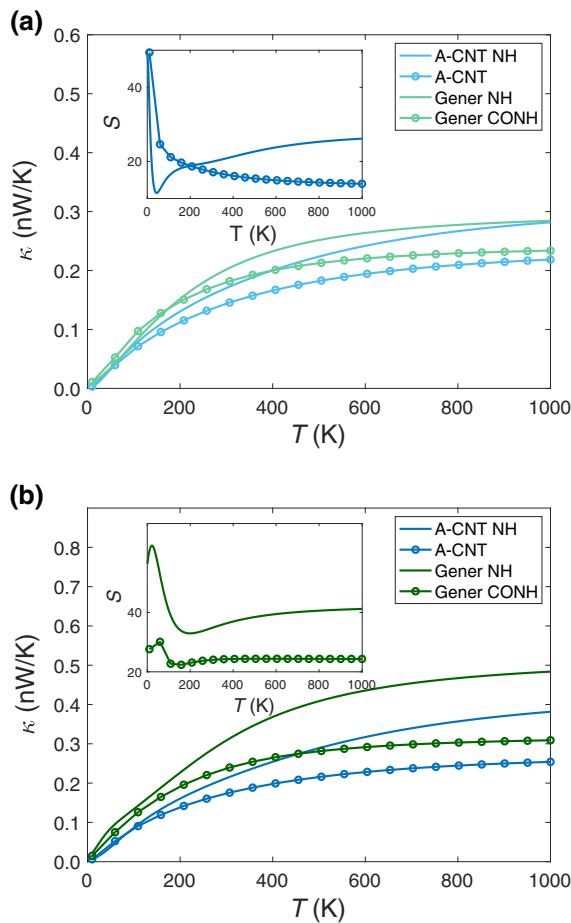


FIG. 10. Conductances of *cis*- (a) and *trans*- (b) isomers, which are connected to armchair-CNT (blue) and generic (green) reservoirs with two different linker groups. The dotted lines correspond to the NHCO linkers. The corresponding switching coefficients are shown in the insets.

Transmission spectra for isomers of azobenzene with three different reservoirs are shown in Fig. 7. Since the generic reservoir supports only the acoustic modes, its bandwidth is narrower than CNT reservoirs. Transmission values for *cis*-azobenzene with the generic reservoir are similar to those with the other reservoirs, but the *trans*-azobenzene generic reservoir yields higher transmission of acoustic modes as expected. Figure 8 shows temperature-dependent conductance and S values of azobenzene junctions with considered reservoir types and a comparison of switching values for azobenzene with different reservoirs at room temperature is available from Table II. Thermal conductance of CNTs increases with diameter. Besides, the generic reservoir model does not include the deformation effect at the linking and folding sites. These factors favor enhanced thermal conductivity values with generic reservoirs and higher S values at all temperatures when compared to CNT reservoirs.

C. Effects of linker groups

In this section, the effects of changing the NHCO linkers with the previous NH groups are investigated. An accompanying difference between two linkers is the extra CO atoms at the contacts [see Fig. 9(b)]. Further, azobenzene molecule is bound to both armchair reservoirs and generic reservoirs by both linkers. Figure 9(a) illustrates the relaxed geometries of the junctions with NHCO linkers. Comparing Figs. 2 and 9, some constitutive variations between the structures are observed. Planar structure of the *trans*-isomer is disturbed, it is slightly bent and the benzene rings are rotated. In addition, the bending direction of the *cis*-isomer is reversed, opposite to the case where azobenzene molecule is bound by the NH linker to armchair CNTs.

Thermal conductance values and switching coefficients are plotted as functions of temperature for *trans*- and *cis*-azobenzene molecules linked to armchair-CNT and generic reservoirs using NH and NHCO linkers in Fig. 10. NHCO linker yields reduced κ and S values compared to the NH linker except for *cis*-isomer at low temperatures. The dihedral angle of *cis*-isomer is 19.311° when bound to armchair CNT by NHCO linkers. Consequently, the additional CO atoms to linker alleviate the stress on bound *cis*-isomer to armchair CNT by NH linker. With NHCO linker and generic reservoir, S is 22%, whereas it is 17% with armchair-CNT reservoir. Remembering that S is 34.78% for generic reservoir with NH linkers, the reduction with use of NHCO is interpreted as being due to the additional CO, which is acting as a barrier for incoming phonons (see Fig. S5).

V. CONCLUSION

In this work, photoisomeric switching of vibrational heat current is studied using junctions built using azobenzene, azobiphenyl, and azotriphenyl molecules. It is observed that the switching coefficient S can be as high as 34.78% at room temperature if the effects of linker groups, reservoir types, and geometrical disturbances can be optimized. S is reduced due to disturbances in the molecular configuration. Still, $S \simeq 20\%$ is possible by using azobenzene with NH linkers at room temperature and $S \simeq 50\%$ at low temperatures such as 10 K. Our findings demonstrate that thermal switching using single molecular junctions could be efficient. The efficiencies can be enhanced further if the geometrical disturbances due to linking to reservoirs can be minimized. Thermal switches investigated here could be realized in a similar way proposed by Del Valle *et al.* [28] for a molecular electronic switch. There, it was suggested to use mobile telescopic multiwalled CNTs, whose low-friction “bamboo” configurations enable a controlled reversible telescoping. The transit time for complete nanotube core retraction was

found to be comparable with the isomerization time of photoactuated molecules, hence making it possible to actualize molecular junctions with mobile carbon-nanotube thermal reservoirs or electrodes.

ACKNOWLEDGMENTS

We acknowledge support from Scientific and Technological Research Council of Turkey (TÜBİTAK) Grant No. 115F445. We are grateful to Ö. Çakır from the Physics Department of İzmir Institute of Technology for fruitful discussions.

-
- [1] N. Li, J. Ren, L. Wang, G. Zhang, P. Hänggi, and B. Li, Colloquium, *Rev. Mod. Phys.* **84**, 1045 (2012).
- [2] L. Wang and B. Li, Phononics gets hot, *Phys. World* **21**, 27 (2008).
- [3] M. Maldovan, Sound and heat revolutions in phononics, *Nature* **503**, 209 (2013).
- [4] L. A. Hart, C. T. Downs, and M. Brown, Keeping it regular: Development of thermoregulation in four tropical seabird species, *J. Therm. Biol.* **64**, 19 (2017).
- [5] M. Fu, W. Weng, W. Chen, and N. Luo, Review on modeling heat transfer and thermoregulatory responses in human body, *J. Therm. Biol.* **62**, 189 (2016).
- [6] C. L. Tan, E. K. Cooke, D. E. Leib, Y.-C. Lin, G. E. Daly, C. A. Zimmerman, and Z. A. Knight, Warm-sensitive neurons that control body temperature, *Cell* **167**, 47 (2016).
- [7] R. Berkowitz, Energy focus automotive industry drives search for tunable thermal switch materials, *MRS Bull.* **42**, 7 (2017).
- [8] E. Paluszak, Z. Chen, G. E. Fernandes, Y. Wan, J. H. Kim, and J. Xu, A thermal diode and novel implementation in a phase change material, *Mater. Horiz.* **2**, 125 (2015).
- [9] E. S. Toberer, L. L. Baranowski, and C. Dames, Advances in thermal conductivity, *Annu. Rev. Mater. Res.* **42**, 179 (2012).
- [10] P. Tao, W. Shang, C. Song, Q. Shen, F. Zhang, Z. Luo, N. Yi, D. Zhang, and T. Deng, Bioinspired engineering of thermal materials, *Adv. Mater.* **27**, 428 (2015).
- [11] X. Gu, Y. Wei, X. Yin, B. Li, and R. Yang, Colloquium: Phononic thermal properties of two-dimensional materials, *Rev. Mod. Phys.* **90**, 041002 (2018).
- [12] N. Li, J. Ren, L. Wang, G. Zhang, P. Hänggi, and B. Li, Colloquium: Phononics: Manipulating heat flow with electronic analogs and beyond, *Rev. Mod. Phys.* **84**, 1045 (2012).
- [13] A. L. Moore and L. Shi, Emerging challenges and materials for thermal management of electronics, *Mater. Today* **17**, 163 (2014).
- [14] S. Narayana and Y. Sato, Heat Flux Manipulation with Engineered Thermal Materials, *Phys. Rev. Lett.* **108**, 214303 (2012).
- [15] S. Neogi, J. S. Reparaz, L. F. C. Pereira, B. Graczykowski, M. R. Wagner, M. Sledzinska, A. Shchepetov, M. Prunnila, J. Ahopelto, C. M. Sotomayor-Torres, and D. Donadio, Tuning thermal transport in ultrathin silicon membranes by surface nanoscale engineering, *ACS Nano* **9**, 3820 (2015).
- [16] Y. Guo and M. Wang, Phonon hydrodynamics and its applications in nanoscale heat transport, *Phys. Rep.* **595**, 1 (2015), phonon hydrodynamics and its applications in nanoscale heat transport.
- [17] M. Maldovan, Phonon wave interference and thermal bandgap materials, *Nat. Mater.* **14**, 667 (2015).
- [18] M.-H. Lu, L. Feng, and Y.-F. Chen, Phononic crystals and acoustic metamaterials, *Mater. Today* **12**, 34 (2009).
- [19] A. A. Balandin and D. L. Nika, Phononics in low-dimensional materials, *Mater. Today* **15**, 266 (2012).
- [20] M. Maldovan, Sound and heat revolutions in phononics, *Nature* **503**, 209 (2013), review article.
- [21] D. Segal and B. K. Agarwalla, Vibrational heat transport in molecular junctions, *Annu. Rev. Phys. Chem.* **67**, 185 (2016).
- [22] S. R. Sklan and J. C. Grossman, Sound and noisy light: Optical control of phonons in photoswitchable structures, *Phys. Rev. B* **92**, 165107 (2015).
- [23] R. Ranganathan, K. Sasikumar, and P. Kebinski, Realizing tunable molecular thermal devices based on photoisomerism is it possible? *J. Appl. Phys.* **117**, 025305 (2015).
- [24] Q. Li, I. Duchemin, S. Xiong, G. C. Solomon, and D. Donadio, Mechanical tuning of thermal transport in a molecular junction, *J. Phys. Chem. C* **119**, 24636 (2015).
- [25] M. Royo, A. Antidormi, and R. Rurrali, A thermal switch for coherent phonons based on a molecular junction, *J. Phys. Chem. C* **121**, 10571 (2017).
- [26] K. Schwab, E. A. Henriksen, J. M. Worlock, and M. L. Roukes, Measurement of the quantum of thermal conductance, *Nature* **404**, 974 (2000).
- [27] L. Cui, W. Jeong, S. Hur, M. Matt, J. C. Klöckner, F. Pauly, P. Nielaba, J. C. Cuevas, E. Meyhofer, and P. Reddy, Quantized thermal transport in single-atom junctions, *Science* **355**, 1192 (2017).
- [28] M. del Valle, R. Gutiérrez, C. Tejedor, and G. Cuniberti, Tuning the conductance of a molecular switch, *Nat. Nanotechnol.* **2**, 176 (2007).
- [29] L. Wang and B. Li, Phononics gets hot, *Phys. World* **21**, 27 (2008).
- [30] D. Porezag, T. Frauenheim, T. Köhler, G. Seifert, and R. Kaschner, Construction of tight-binding-like potentials on the basis of density-functional theory: Application to carbon, *Phys. Rev. B* **51**, 12947 (1995).
- [31] G. Seifert, D. Porezag, and T. Frauenheim, Calculations of molecules, clusters, and solids with a simplified LCAO-DFT-LDA scheme, *Int. J. Quant. Chem.* **58**, 185 (1996).
- [32] M. Elstner, D. Porezag, G. Jungnickel, J. Elsner, M. Haugk, T. Frauenheim, S. Suhai, and G. Seifert, Self-consistent-charge density-functional tight-binding method for simulations of complex materials properties, *Phys. Rev. B* **58**, 7260 (1998).
- [33] G. Seifert and J. O. Joswig, Density functional tight binding an approximate density functional theory method, *Wiley Interdiscip. Rev. Comput. Mol. Sci.* **2**, 456 (2012).
- [34] B. Aradi, B. Hourahine, and T. Frauenheim, Dftb+, a sparse matrix-based implementation of the dftb method, *J. Phys. Chem. A* **111**, 5678 (2007).

- [35] H. Chermette, Chemical reactivity indexes in density functional theory, *J. Comput. Chem.* **20**, 129 (1999).
- [36] F. De Proft and P. Geerlings, Conceptual and computational dft in the study of aromaticity, *Chem. Rev.* **101**, 1451 (2001).
- [37] M. Elstner, D. Porezag, G. Jungnickel, J. Elsner, M. Haugk, T. Frauenheim, S. Suhai, and G. Seifert, Self-consistent-charge density-functional tight-binding method for simulations of complex materials properties, *Phys. Rev. B* **58**, 7260 (1998).
- [38] G. Kresse and J. Furthmüller, Efficient iterative schemes for ab initio total-energy calculations using a plane-wave basis set, *Phys. Rev. B* **54**, 11169 (1996).
- [39] J. P. Perdew, K. Burke, and M. Ernzerhof, Generalized Gradient Approximation Made Simple, *Phys. Rev. Lett.* **77**, 3865 (1996).
- [40] J. M. Soler, E. Artacho, J. D. Gale, A. García, J. Junquera, P. Ordejón, and D. Sánchez-Portal, The SIESTA method for ab initio order-n materials simulation, *J. Phys.: Condens. Matter* **14**, 2745 (2002).
- [41] M. del Valle, R. Gutierrez, C. Tejedor, and G. Cuniberti, Tuning the conductance of a molecular switch, *Nat. Nano. Sci.* **2**, 176 (2007).
- [42] T. Yamamoto and K. Watanabe, Nonequilibrium Green's Function Approach to Phonon Transport in Defective Carbon Nanotubes, *Phys. Rev. Lett.* **96**, 255503 (2006).
- [43] A. Ozpineci and S. Ciraci, Quantum effects of thermal conductance through atomic chains, *Phys. Rev. B* **63**, 125415 (2001).
- [44] H. Sevinçli, S. Roche, G. Cuniberti, M. Brandbyge, R. Gutierrez, and L. M. Sandonas, Green function, quasi-classical Langevin and Kubo–Greenwood methods in quantum thermal transport, *J. Phys.: Condens. Matter* **31**, 273003 (2019).
- [45] L. Chaput, A. Togo, I. Tanaka, and G. Hug, Phonon-phonon interactions in transition metals, *Phys. Rev. B* **84**, 094302 (2011).
- [46] A. Togo and I. Tanaka, First principles phonon calculations in materials science, *Scr. Mater.* **108**, 1 (2015).
- [47] G. Srivastava, *The Physics of Phonons* (Taylor & Francis, New York, 1990).
- [48] M. P. L. Sancho, J. M. L. Sancho, J. M. L. Sancho, and J. Rubio, Highly convergent schemes for the calculation of bulk and surface Green functions, *J. Phys. F: Metal Phys.* **15**, 851 (1985).
- [49] See Supplemental Material at <http://link.aps.org/supplemental/10.1103/PhysRevApplied.14.064045> for additional information concerning systems, vibrational properties of azobenzene [51], mode analysis, and implementation of generic reservoirs [52].
- [50] H. Sevinçli, T. Lehmann, D. A. Ryndyk, and G. Cuniberti, Comparison of electron and phonon transport in disordered semiconductor carbon nanotubes, *J. Comput. Electron.* **12**, 685 (2013).
- [51] N. Biswas and S. Umapathy, Density functional calculations of structures, vibrational frequencies, and normal modes of trans- and cis-azobenzene, *J. Phys. Chem. A* **101**, 5555 (1997).
- [52] W. Müller, R. Schiller, and W. Nolting, Understanding of surface states in a correlated electron system, *Eur. Phys. J. B: Condens. Matter Complex Syst.* **16**, 705 (2000).